



The Ultimate Pattern of Shock-Vortex Interaction

Keun-Shik Chang*, Hrushikesh Barik* and Se-Myong Chang**

*Departmrnt of Mechanical & Aerospace Engineering Systems, KAIST

** Department of Mechanical Engineering, Kunsan National University

Abstract: As a shock impinges into a vortex of variable strength, complex shock diffraction can occur. Since a vortex has a fixed rotating direction, the shock wave travelling in one direction creates strong asymmetry in the vortex flow field. The process is that first the shock is divided into two parts by the vortex. One part is moving in the adverse direction opposite to the vortex flow which is captured by the vortex center. The other part is moving in the favorable direction, namely, in the direction same as the vortex flow; it is swung around the vortex, accelerating the vortex flow. In this paper we have investigated numerically using ENO scheme how and why the shock-vortex interaction patterns appear so different for different parametric values. Conclusion is that there are three different types of shock-vortex interaction depending on two related parameters: shock Mach number and vortex Mach number. We present a parameter map by which we can discern what type of interaction pattern appears as a shock impinges into a vortex.

1. INTRODUCTION

It is well known that turbulent flow creates vortices in the boundary layer. As a shock travels in vortex-ritten turbulent flow, it can create much shock-vortex interactions and acoustic noises. The shock interacting with the vortex can create secondary and even tertiary shocks and as many vortices and slip lines. The process is in overall called shock diffraction phenomena which must be properly understood for better design of flight vehicles and propulsion engines in the compressible flow regime.

The current work presents classification of the shock-vortex interaction in a quantitative manner. We present a parameter map by which we can discern what type of interaction can occur. The interaction has three types depending on two parameters, shock Mach number and vortex Mach number. Type I is for the under-developed interaction with neither induced shock in the vortex nor reflected shock from the vortex edge. Type III represents the fully-developed shock-vortex interaction with both induced shock and reflected shocks clearly visible due to vortex flow of supersonic speed. The shocks are in bipolar structure and the reflected shock has either RR(Regular Reflection), MR(Mach Reflection) or DMR (Double Mach Reflection) structure. Type II is, in contrast, for the shock-vortex interaction with shock reflection still developing. We have physically elaborated how the interaction model changes from Type I to Type II and Type III as the interaction becomes much stronger. This work is the extension of earlier work by the present authors[5].

2. NUMERICAL METHOD AND VORTEX MODEL

We employed a high resolution shock-capturing scheme, the third-order Essentially Non-Oscillatory (ENO) scheme[3-4] to solve the unsteady Euler equations. ENO schemes can resolve complex aeroacoustic fields containing both shock and acoustic waves.

The compressible vortex in the present work is similar to that described by Ellzey[1]. The vortex model consists of two region: an inner core region represented by

$$U_\theta(r) = \frac{U_c r}{R_c}, \quad r < R_c \quad (1)$$

and an outer distribution given as

$$U_\theta(r) = Ar + \frac{B}{r}, \quad R_c \leq r \leq R_0 \quad (2)$$

where, U_θ = tangential velocity, U_c = constant core velocity, r = distance from the vortex center, R_c = core radius, and R_0 = outer radius. The coefficients A and B in the Equation (2) are chosen so that $U_\theta = U_c$ when $r = R_c$ and $U_\theta \rightarrow 0$ when $r = R_0$. Outside $r = R_0$, the velocity is zero everywhere. The initial pressure is always specified such that the pressure gradient balances the centripetal force as in

$$\frac{\partial p}{\partial r} = \rho \frac{U_\theta^2}{r} \quad (3)$$

In this work, a planar shock travels from right to left to interact with a stationary compressible vortex rotating counterclockwise. The computational domain for these calculation is 10cm×10cm and consists of 960×960 uniform grid. The initial conditions behind the shock wave are prescribed according to Rankine-Hugoniot relations while ambient conditions are given elsewhere. For all open boundaries, conventional characteristic boundary conditions based on Riemann invariants are prescribed[2].

3. THREE SHOK-VORTEX INTERACTION MODELS

In the present work, interaction of a shock wave with an isolated compressible vortex has been simulated for a range of incident shock Mach number (M_s) and vortex Mach number (M_v). The maximum M_s 1.6 and the maximum M_v is 1.2.

In Fig. 1, Type I shock-vortex interaction is presented. Here, we have chosen a rather low shock Mach number, $M_s=1.2$, and subsonic vortex Mach number, $M_v=0.7$. The shock is first deformed by the vortex before it is disconnected: see Fig.1(a). The upper part of the shock is swung around the vortex. It helps accelerating the rotational flow in the upper region of the vortex. The vortex flow, however, never reaches locally supersonic in the Type I interaction. The lower part of the shock is captured at the vortex center and the shock strength is weak as it rotates clockwise against the vortex flow. The captured shock and the accelerated shock makes shock-shock interaction, first RR type and later MR type with two weak slip lines emanated from the triple points that merges with the vortex in a spiral form.

It results in quite uneven and asymmetric distribution of kinematic and thermodynamic variables in the vortex. Fig. 2

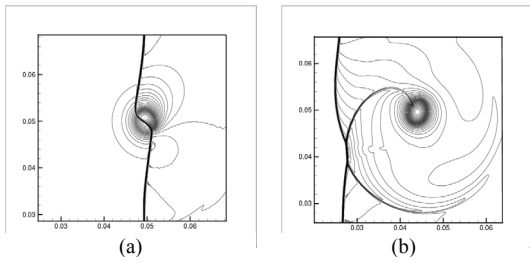


Fig. 1 Density contours at two time steps (a-b); Type I ($Ms=1.2$ & $Mv=0.7$).

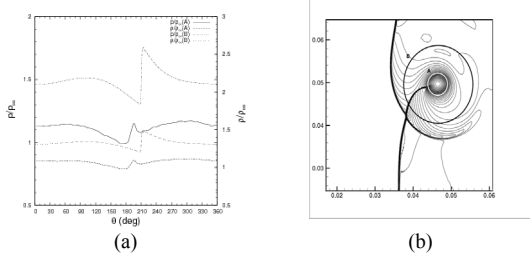


Fig. 2 (a) Non-dimensional circumferential pressure and density variation on two circles A and B for Type I ($Ms=1.2$ & $Mv=0.7$), (b) location of two circles (A, B)

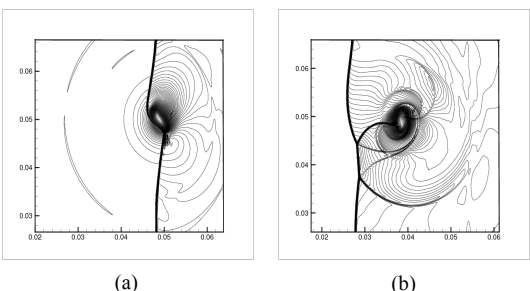


Fig. 3 Density contours at two time steps (a-b); Type III ($Ms=1.6$ & $Mv=1.0$).

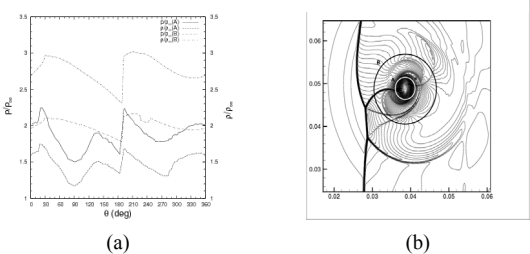


Fig. 4 (a) Non-dimensional circumferential pressure and density variation on two circles A and B for Type III ($Ms=1.6$ & $Mv=1.0$), (b) location of two circles (A, B).

demonstrates that, along the circumferential direction of two imaginary circles A (inside the vortex) and B (outside of the vortex), density or pressure value jumps high after a single shock near $\Theta=210$ (Θ is anticlockwise and $\Theta=0$ is eastward) before it is lowered back to the periodic condition. It is noted that the travelling shock in the vortex is just moving in a subsonic flow.

Fig. 3 shows computed results for shock vortex interaction of Type III with $Ms=1.6$ and sonic vortex Mach number,

$Mv=1.0$. Acceleration of the flow by the upper part of shock wave is more severe, making the vortex flow supersonic everywhere. The flow and shock waves appear almost rotationally symmetric in and near the vortex. Opposite to the captured shock, there is a fully developed shock wave induced by the captured shock, making the vortex flow appear rather rotationally symmetric and of dipole structure. The triple points on the Mach stem of shock-shock interaction produce much stronger slip lines that spiral into the vortex. Density and pressure distribution in Fig. 4 show existence of two shocks and dipole type of pressure sources.

The captured shock in Fig. 3 shows that it is reflected from the vortex edge in MR type with a weak slip line. The vortex appears now no more a circle but an elongated form. Opposite to the captured shock, it is observed that there is an induced shock developing in time. First it is small but soon grows mature with its own reflected shock from the vortex edge and a slip line from the triple point. In Type I interaction, this was not possible because the vortex flow was purely subsonic. In type III, the captured shock is a traveling shock as in Type I. But the induced shock is like a stationary shock created in a supersonic flow. As the captured shock rotates clockwise, the induced shock also rotates in the opposite direction. As the captured shock develops a reflected shock, the induced shock also develops a reflected shock.

Why does the nature choose such rotational symmetry? The answer seems as follows. A vortex should consume least energy when the flow is concentric. When a strong shock approaches, the vortex is elongated and the flow can be no more concentric. By capturing a shock wave, the vortex further has a monopole pressure source making the vortex severely biased in circumferential distribution. Dynamic vector variables like velocity, acceleration, vorticity, force and momentum are all biased in addition to the thermodynamic scalar variables like density, pressure, entropy, enthalpy and stagnation pressure. If the flow were of dipole structure with all the variables having nearly rotationally-symmetric distribution, the vortex flow would be dynamically much better balanced. It could perhaps be compared to wheel balancing of a high speed racing car in order to reduce possible wobbling of a tire. To stabilize the vortex, an induced shock is developed for dynamic balance: it gives almost a rotational symmetry opposite to the captured shock. The symmetry includes not only the induced shock but also its reflected shock and slip line. Depending on the strength of the shock (or vortex), the reflected shock can be either RR, DR or even DMR type.

In Fig. 5, shock-vortex interaction of Type II is shown with $Ms=1.4$ and $Mv=0.8$. Here the counterclockwise vortex flow is subsonic initially but accelerated to supersonic speed locally by the aid of upper part of the incident shock. Interaction of Type II in Fig. 5 appears similar to Fig. 1 at a first glance. As we examine more closely Fig. 5, however, there are some acoustic waves weakly developing in the opposite direction to the captured shock. The pressure and density distribution in the circumferential direction in Fig. 6 also confirms this: compression wave begins to develop, near $\Theta=40$ degree, opposite to the captured shock at $\Theta=210$ degree. These waves will develop to a shock wave should the vortex flow be accelerated to entirely supersonic flow with shock wave or vortex flow stronger than the present case.

The three types of shock-vortex interaction are summarized by schematic diagram in Fig. 7. They all show the incident shock(I1, I2, and I3), Mach stem(I3) of the shock-shock interaction with its two slip lines(s1 and s2) spiraling to the vortex, the frontier shock(I4) catapulted from the upper part of the incident shock and enclosing the disturbed pressure

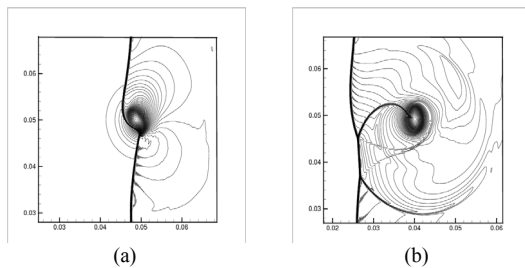


Fig. 5 Density contours at two time steps (a-b); Type II (Ms=1.4 & Mv=0.8)

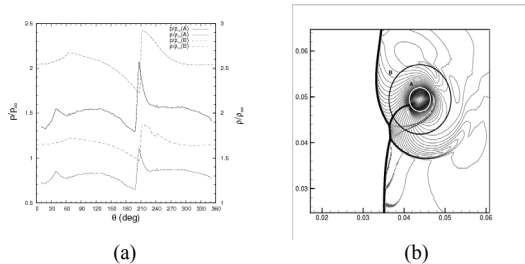


Fig. 6 (a) Non-dimensional circumferential pressure and density variation on two circles A and B for Type II, Ms=1.4, Mv=0.8 (b) location of the radii (A, B)

field radiating from the vortex, and the captured shock(I5) attached to the vortex. Type I interaction shows no induced wave from the incident shock, neither acoustic waves nor a shock wave. Type II shows weak induced wave(I6) of acoustic pressure level. Type III is the most complicated, with a pair of rotationally symmetric wave structures in the vortex. The captured shock(I5) has a reflected

shock(I6) and a slip line(s3), and the induced shock has its counterparts(I7 and I8 with s4). All the slip lines spiral into the vortex. Type I (left of the central confined region), Type II (central confined region), and Type III (right to the central confined region). Axis is vortex Mach number and ordinate is shock Mach number. The symbol marks are those parameter points investigated experimentally or computationally by other researchers.

Fig.8 shows a Ms-Mv Map from which we can tell what type of shock-vortex interaction occurs for a given set of shock and vortex Mach numbers. We have calculated 42 parameter cases and identified what interaction type they belong to by inspecting the circumferential pressure and density distribution. The curves corresponding to Type II developed acoustic waves but showed no evidence of induced shock wave. The curves of Type I showed no evidence of acoustic waves at all.

4. CONCLUSION

Shock-vortex interaction patterns have been classified into three types depending on how much the induced shock is developed opposite to the captured incident shock. In this way, we were able to eliminate the qualitative character of the conventional terminology like 'weak or strong shock-vortex interactions'. A parameter map has been presented in the plane of shock and vortex Mach numbers. It must be very useful in distinguishing the type of shock-vortex interaction expected for a given pair of parameters. The reason and patterns of induced-shock development have been elaborated. In this way,

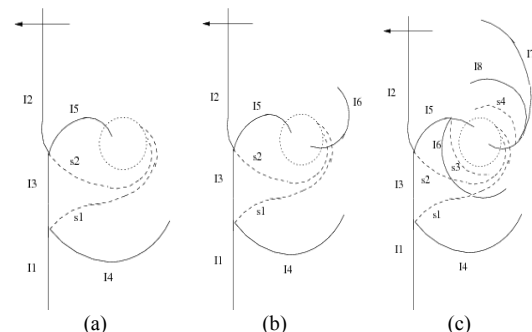


Fig. 7 Schematic diagrams for shock-vortex interaction: (a) Type I, (b) Type II, and (c) Type III.

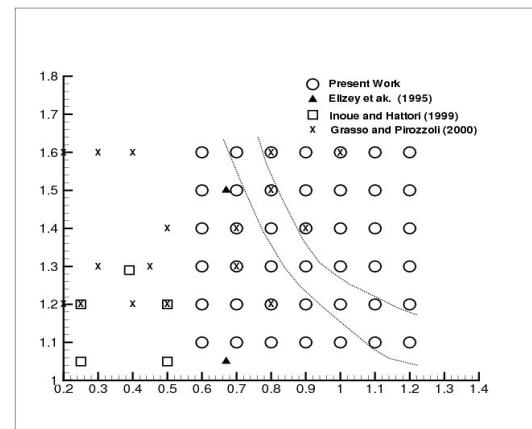


Fig. 8 A parameter map for shock-vortex interaction.

we have been possible to understand better why the shock-vortex interaction takes particular structured pattern although they may appear complicated. The present knowledge on shock diffraction behavior due to vortex should be beneficial to those researchers trying to improve noise and efficiency characteristics of the flight vehicles and engines.

REFERENCES

- [1] 1995, Ellzey, J.L., Henneke, M.R., Picone, J.M. and Oran, E.S., "The interaction of a shock with a vortex: Shock distortion and the production of acoustic waves," *Phys. of Fluid*, Vol.7, pp.172–183.
- [2] 1999, Chatterjee, A., "Shock waves deformation in shock-vortex interactions," *Shock Waves*, Vol.9, pp.95–105.
- [3] 1988, Shu, C.W. and Osher, S., "Efficient implementation of essentially non-oscillatory shock-capturing schemes," *Journal of Computational Physics*, Vol.77, pp.439–471.
- [4] 1989, Shu, C.W. and Osher, S., "Efficient implementation of essentially non-oscillatory shock-capturing schemes, ii." *Journal of Computational Physics*, Vol.83, pp.32–78.
- [5] 2004, Chang, S.-M., Chang, K.-S. and Lee, S., "Reflection and Penetration of Shock Wave Interacting with a Starting Vortex," *AIAA Journal*, Vol.42, No.4, pp.796–805.